Diameter dependence of the UV light detecting performance of InGaN/GaN nanorods array photodetector

Yunlong Kang[1], Ding Wang[1,2], Ping Wang[1,2], Aiying Chen[1], Huijun Li[1], Xianying Wang[1,2] ✉, Junhe Yang[1,2]

[1]*School of Materials Science and Engineering, University of Shanghai for Science & Technology, Shanghai 200093, People's Republic of China*
[2]*Shanghai Innovation Institute for Materials, Shanghai 200444, People's Republic of China*
✉ *E-mail: xianyingwang@usst.edu.cn*

Published in Micro & Nano Letters; Received on 24th February 2018; Revised on 12th May 2018; Accepted on 21st June 2018

Vertically aligned InGaN/GaN nanorod arrays with multiple quantum wells (MQWs) was prepared via inductively coupled plasma (ICP) followed by a further anisotropic wet etching method. It was demonstrated that the sizes of nanorods could be easily regulated in the ranges of 330–1090 nm by simply controlling the ICP etch parameters. The morphology characterisation results indicated that these nanorods are of straight and smooth appearance, and the length of nanorods is about 4 μm. Ultraviolet (UV) detectors based on nanorods arrays with different diameters were fabricated, which exhibited fast response/recovery speed and good response. The UV detecting performance was getting better with the decrease of nanorods diameter, which may be caused by the suppression of the dark current. This work provides an efficient route for fabricating the large-scale vertical aligned MQWs nanorods array and developing their fascinating applications.

1. Introduction: InGaN/GaN multiple quantum wells (MQWs) have been intensively studied as materials for visible and ultraviolet (UV) light emission and detection [1]. Due to the large lattice mismatch between InN and GaN, strain-induced piezoelectric fields along the *c*-direction are generated across the InGaN/GaN MQWs, causing the quantum-confined Stark effect [2]. The performance of InGaN/GaN MQWs devices is negatively affected by the presence of a large number of threading dislocations and the strong internal polarisation field in c-oriented thin films [3]. The low-dimensional nanomaterials present promising advantages for photodetectors because of the independent optimisation of light absorption, the carrier collection and the efficient light trapping, thus leading to a possibility to reduce the active material volume without losing efficiency [4]. Compared with the conventional film structure, the dislocation density of nanowires/nanorods array is drastically reduced due to the free lateral surface, which allows efficient relaxation of the lattice misfit strain [5]. Furthermore, semiconductor nanorods usually display good device performance due to their strong light trapping effect, which have been confirmed by theoretical simulation based on finite difference time domain approach [6–8].

GaN or InGaN/GaN nanowires/nanorods array is prepared commonly using in 'bottom-up' synthetic methods such as metal-organic chemical vapour deposition (MOCVD), molecular beam epitaxy, chemical vapour deposition (CVD) and so on [9–11]. Recently, some research groups have prepared the GaN nanowire with the 'top-down' method because it is propitious in large scale manufacture [12]. Owing to the fact that different components of the III nitride material have different surface potentials, which will generate different etching speed, it is difficult to obtain the structure with the smooth side wall. In order to solve this problem, it is very important to fabricate GaN devices with high quality nanorod structures, and this study has shown a research for fabricating large area GaN nanodevices through dry and wet etching.

Herein, vertically aligned InGaN/GaN MQWs nanorods array was prepared via a two-step etch approach, which includes an inductively coupled plasma (ICP) etch and a further anisotropic wet etching. The morphological and structural characters of materials are analysed. In addition, the current–voltage (*I–V*) characteristics of the photodevices are measured to study the UV detecting performance. The response value and response–recovery time are analysed through the response–recovery characteristic curves to identify whether the showed diameter of nanorods improves the detecting performance.

2. Experimental section

2.1. Preparation of InGaN/GaN MQW film: The InGaN/GaN MQW epitaxial thin film was grown on the c-plane sapphire with MOCVD method. The sources of gallium (Ga), indium and nitrogen (N_2) were trimethylgallium, trimethylindium and ammonia (NH_3), respectively. The n-type and p-type doping was accomplished by Si and Mg doping with silane (SiH_4) and dicyclopentadienyl magnesium as a source. Typically, after cleaning the sapphire wafer, an intrinsic GaN (u-GaN) epitaxial layer was first deposited onto the substrate by MOCVD. The thickness of the intrinsic GaN epitaxial layer was measured to be 3 μm. Then, an n-GaN epitaxial layer of 1.5 μm was formatted by Si doping. Afterwards, a five paired superlattice structure of $In_{0.11}Ga_{0.89}N$/GaN with a thickness of ~2/16 nm was deposited. Subsequently, another 200 nm epitaxial p-GaN layer was obtained with Mg doping.

2.2. Preparation of InGaN/GaN nanorods array: InGaN/GaN nanorods array was fabricated via a 'top-down' two-step etch approach. Figs. 1*a–e* illustrated the schematic of formation processes of InGaN/GaN nanorods array. First, a SiO_2 mask layer with the thickness about 1 μm was grown by CVD method (Fig. 1*b*). Then, photolithographic technology was used to form a circular pattern with the diameter about 5 μm and then Buffered Oxide Etch (BOE) technology was used to corrode the SiO_2 mask layer to form an etching mask with the diameter about 1 μm. The pattern of the SiO_2 mask was used for the next dry etch step (Fig. 1*c*). The epitaxial layer of GaN was etched by ICP etching with the ICP source power and gas flow rate were 800 W and 30 sccm, respectively. The diameter of nanorods was controlled by adjusting the RF chuck power from 70 to 100 W (Fig. 1*d*). After the dry etch, tapered-shaped nanostructures were formed with severe surface damage and roughness. Then, a KOH-based solution (AZ400K) was utilised to selectively wet

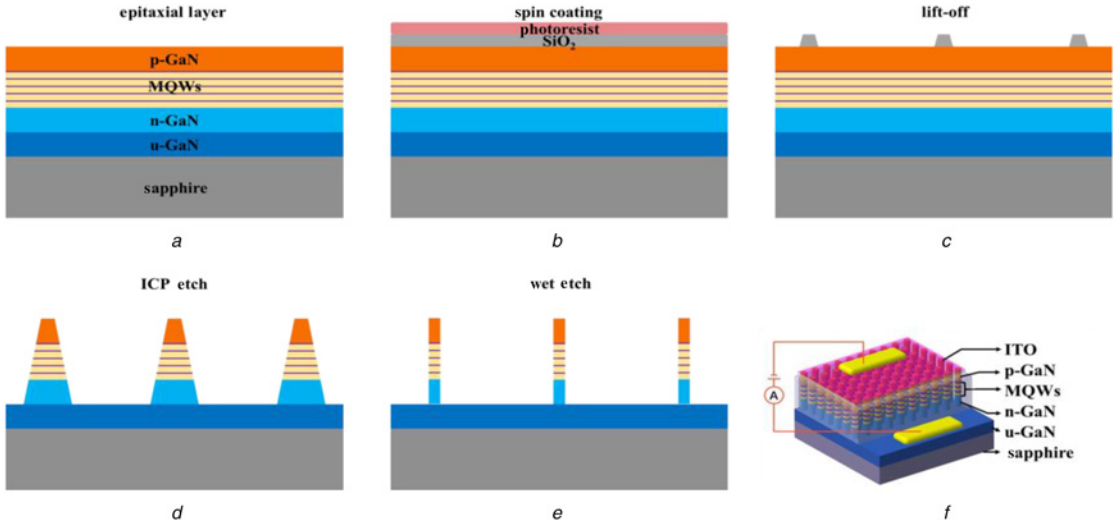

Fig. 1 *Schematic diagram of formation processes of InGaN/GaN nanorods array*
a Grown epitaxial layer on sapphire (0001) by MOCVD
b Fabricated the SiO_2 layer by CVD and spin coated the photoresist on the SiO_2 layer
c Photolithographic of the mask pattern, BOE of SiO_2 and lift-off of the photoresist
d ICP etching InGaN/GaN microstructure
e Formation microrods array by wet etch
f Illustration schematic of the UV detector

etching structures in order to obtain the straight, vertical and smooth nanorod (Fig. 1*e*).

2.3. Fabrication of InGaN/GaN nanorods array detector: The schematic diagram and the fabricating process of the device were shown in Fig. 1*f*. Polymethylmethacrylate with a thickness of 6 µm was filled in nanorods array and it was cured at room temperature for 24 h, and the side wall of the nanorods was passivated and protected. Then, the nanorods were etched with ICP to expose the p-GaN. A layer of ITO with 200 nm was sputtered on the P-GaN. Afterwards, a 200 nm Au layer was deposited on both ends as electrodes via electron beam evaporation (Fig. 1*f*'). Electronic properties of the device were tested by using a semiconductor characterisation system (Keithley, 4200-SCS, USA). The light of 365 nm from an UV lamp (12 W, ZF-7, Gongyi City Yuhua Instrument Co., Ltd., Henan Province, China) was used as UV source. The light source (from a 365 nm with the power density of 0.3 mW/cm^2) was placed 10 cm away from the nanodevice. The response ($s = I_{UV}/I_{dark}$) of the sensor was defined as the ratio of detector electric current under UV irradiation (I_{UV}) to that in the dark (I_{dark}). The time is taken by the detector which ranged from I_{dark} to $I_{dark} + 90\%$ ($I_{UV} - I_{dark}$) was defined as the response time when the detector was exposed to the UV light. The time is taken by the detector which changed from I_{UV} to $I_{UV} - 90\%$ ($I_{UV} - I_{dark}$) was defined as the recovery time when the detector was retrieved from the UV light. Responsivity (R) and specific detectivity (D^*) are two critical parameters employed to evaluate the sensitivity of a detector, the responsivity (R_λ) of the device is calculated using the method in [13].

2.4. Characterisations methods: The morphology of the InGaN/GaN nanorods array was characterised by field-emission scanning electron microscopy (FE-SEM, FEI, Quanta FEG). The InGaN/GaN nanorods were removed from the sapphire substrate by the ultrasonic treatment and then collected for the high-resolution transmission electron microscopy (HR-TEM) analysis. TEM, HR-TEM and selected area electron diffraction (SAED) images were recorded with a Tecnai G220S-Twin transmission electron microscope operating at an accelerating voltage of 120 and 200 kV, respectively. To investigate the optical properties of InGaN/GaN nanorods array, the room temperature PL spectra measurements were carried out by using LabRAM HR Evolution (Horiba, LabRAM HR Evolution, France) with a He-Cd laser 325 nm as the excitation light. The spectral photoresponses of the photodetectors were analysed with a Xe lamp, monochromator, a program-controlled semiconductor characterisation system (Keithley 4200-SCS, USA) [14].

3. Results and discussions

3.1. Morphology characterisations of InGaN/GaN nanorods array: The morphologies of the fabricated InGaN/GaN nanorods array were characterised by FE-SEM. Fig. 2 displays the regularly arranged large scale of InGaN/GaN nanosturctures after ICP etch and the tilt-view FE-SEM image of the more distinct morphology structure. After ICP etching, there forms the circular truncated cone on the sapphire. As shown in Fig. 2, the etch depth is approximately similar to the different ICP parameters. However, the top diameter of the cone can be controlled by adjusting the ICP etching parameters. As reported by Lee [15], the ion power density of plasma is dependent on the ion energy and ion density, which were affected by ICP source power, RF chuck power, chamber pressure and gas flow rate. The ion power is the decisive factor that influences the etch rate of materials. In this work, the regulation of nanorods diameters by RF chuck power shows excellent agreement with the report.

The InGaN/GaN nanorods array was fabricated by further anisotropic wet etching of GaN microtruncated-pyramid. With this etchant, the top Ga-polar c-plane surface has a near zero etch rate while the {10-10} *m*-plane sidewalls have a relatively fast etch rate compared to the other planes [16]. Fig. 3 shows the FE-SEM images of the InGaN/GaN nanorods array, which have a straight and smooth sidewall. Fig. 3 indicates the regularly arranged nanorods array with different diameters can be fabricated on a large scale. The length of the nanorod is about 4 µm, and the diameters are about 330, 460, 730 and 1090 nm, respectively. Different diameters are depended on RF chuck power. Therefore, the ICP etch technique could adjust the formation of a smaller diameter and more steep side walls for fabricating the straight and smooth nanorods and could avoid different wet etching rates.

doi: 10.1049/mnl.2018.5160

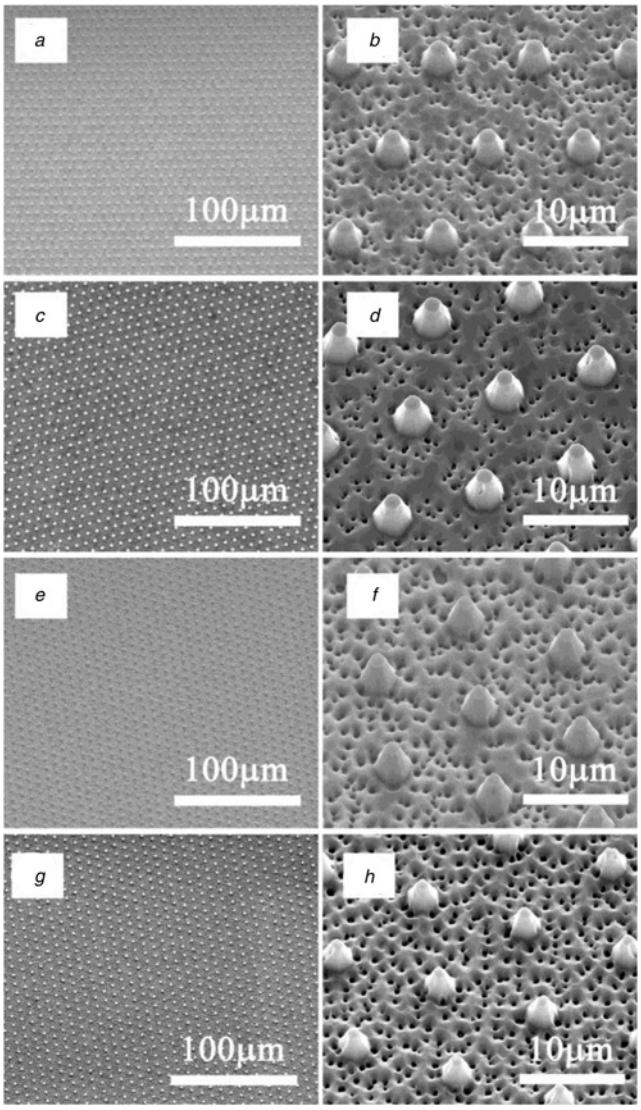

Fig. 2 *SEM images of different diameter InGaN/GaN MQWs nanostructure after ICP etching with different RF chuck power*
a, *b* 70 W
c, *d* 80 W
e, *f* 90 W
g, *h* 100 W

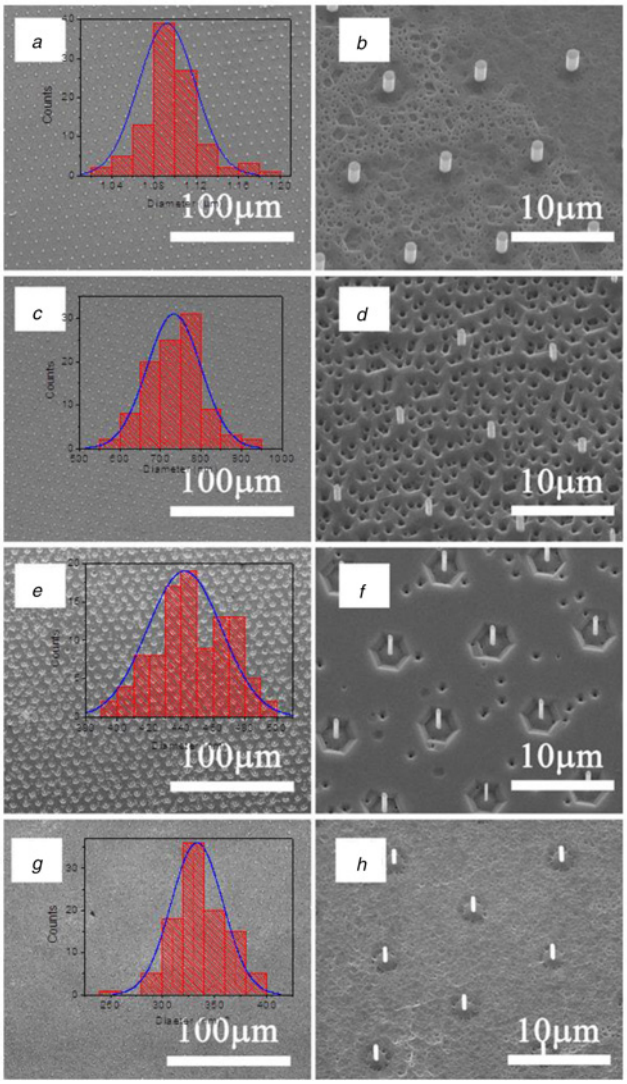

Fig. 3 *FE-SEM images of different diameter InGaN/GaN MQWs nanostructure after wet etching with a tilt of 20°*
a, *b* 1090 nm
c, *d* 730 nm
e, *f* 460 nm
g, *h* 330 nm

The large-scale controllable preparation method and the controllable diameters have the potential for industrial production applications.

The crystal structure and morphology of InGaN/GaN MQW nanorods were further revealed by TEM. Fig. 4*a* shows a TEM image of the InGaN/GaN nanorod fabricated with the 'top-down' method on sapphire substrates which was obtained by ultrasonic processing the array in ethanol. The representative nanorod has straight and smooth surface. In addition, the length and the diameter of InGaN/GaN nanorods are ∼4 μm and 300 nm, respectively, which is consistent with the FE-SEM characterisation in Fig. 3*g*. As shown in Fig. 4*b*, it is observed that the thickness of the InGaN/GaN MQW nanorod is almost uniform throughout the five periods. Five pairs of InGaN/GaN MQW are clearly seen and are evenly distributed among the n-GaN. Energy dispersive X-ray spectroscopy linear scanning of the InGaN/GaN MQW NW region clearly confirms the spatial distributions of In in the nanorod structure. The thickness of the InGaN and GaN MQW is estimated to be 2 and 16 nm, respectively. Fig. 4*c* shows the HR-TEM image of InGaN/GaN MQW nanorod. It is evident that the growth direction of the nanorod is the [0001], which is aligned along the nanorod axis. The lattice is completely perfect without any defects. No stacking faults or dislocations are observed in the InGaN/GaN MQW nanorod structure. The interplanar spacing of the GaN nanorod segment measured from the HR-TEM image is about 2.6 Å. The clear SAED spots and HRTEM image indicated that the GaN nanorod is single crystalline with a wurtzite structure and a growth direction of ⟨0001⟩. The high-quality InGaN/GaN nanorod structures were attributed to the selective KOH-based wet etching. As the report [17], on the (0001) Ga-polar facet, the surface is converted into N-terminated with three electronegative dangling bonds when the first Ga layer is removed by OH ions. Due to the large repulsive force between the three electronegative dangling bonds and OH ions, the OH ions are unable to access the surface. For this reason, the (0001) Ga-polar facet is resistant to the wet-etching in KOH solution. Therefore, KOH solution can selectively etch the {1101} N-polar sidewalls while leave the (0001) Ga-polar top surface intact. A representative SAED pattern is shown in Fig. 4*d*, where (0-110), (000-1), (0001) and (01-10) diffraction crystal planes are present.

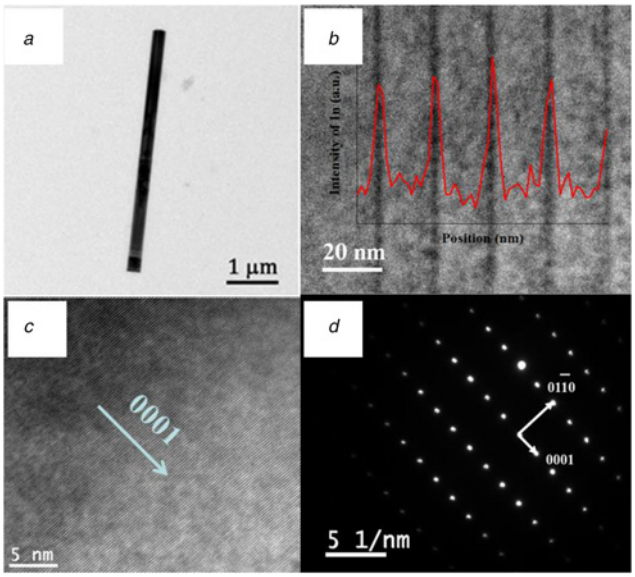

Fig. 4 *Morphology and composition characterisation of the InGaN/GaN MQWs nanorod*
a, *b* TEM and indium composition of the InGaN/GaN MQWs nanorod
c HR-TEM images of the InGaN/GaN MQWs nanorod
d SAED pattern of the MQWs nanorod

3.2. PL spectra of InGaN/GaN nanorods array: Fig. 5*a* is the PL spectra curves of samples in different fabrication steps. Double emission peaks at 423 and 452 nm were observed for the InGaN/GaN MQWs film. After etching by ICP, the strong emission peak at 361.3 nm is observed and the peaks in the blue spectral range (peaks occurring at 423 and 452 nm) are almost disappeared. MQW PL emission is prominent only for the unprocessed film and after processing/etching, the only PL signal left is that due to the GaN band edge emission. For the etched pillars, the quantum well luminescence is strongly quenched. It means that the MQWs layer is damaged by the top-down approach, likely due to the creation of surface states that act as efficient non-radiative recombination centres. In addition, the destruction of the MOWs layer results in the exposure of GaN. After further wet etching, the full width at half maximum obviously reduces and the position of emission peak has low blue shifts, which is attributed to the further releasing of internal stress of the material [18]. Fig. 5*b* exhibits the PL spectra of different diameter of InGaN/GaN MQWs nanorods array. The room temperature PL spectra of the InGaN/GaN MQWs nanorods array are 363.5, 362.4, 361.9 and 361.3 nm for the nanorods diameters of 1090, 730, 460, and 330 nm, respectively. The peaks of the InGaN/GaN MQWs nanorods array exhibit weak blue shift with the decrease of nanorods diameter. The reason for the blue shift cannot be the quantum size effect, because the diameters of prepared GaN nanorods are bigger than GaN exciton Bohr radius between 2.8 and 3.5 nm [19], which exceed the scale worked

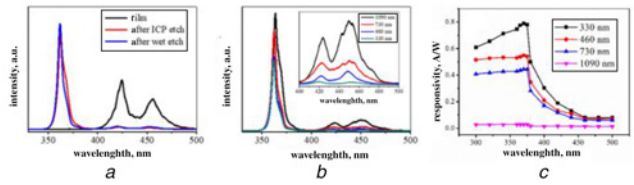

Fig. 5 *Room temperature PL properties*
a PL spectra of InGaN/GaN nanorods array at different preparation steps
b PL spectra of InGaN/GaN nanorods array with different diameters
c Comparison of responsivity of InGaN/GaN nanorods arrays with various diameters at a bias of 0.5 V

by the quantum confinement effect. Therefore, the strain relaxation of the InGaN/GaN MQWs nanorods array should undertake major responsibilities for the blue shift. The double emission peaks at 423 and 452 nm are decreased with the smaller of diameter in the illustration of Fig. 5*b*. For this work, the decrease in PL intensities for nanorods with smaller diameters can be attributed to the following reasons: First, the active area of the InGaN/GaN nanorods array (total emission area of the InGaN/GaN nanorods array emission area) is decreased with the diameter [18]. Second, the strain relaxation is benefit to enhance electron–hole wave function overlap and lead to a higher recombination rate for smaller nanorods. Third, the surface/volume ratio becomes larger as the diameter decreases, and the light form smaller diameter can be emitted more easily through the sidewall than that form the larger ones. Therefore, the combination of the above factors results in the decrease in PL intensities for nanorods with smaller diameters. The trend of independent PL emitting peaks will lead to a more important application in optoelectronic devices, such as the LED, laser source, photodetectors and so on.

3.3. Spectral photoresponse of InGaN/GaN nanorods array: As mentioned before, the diameter of InGaN/GaN QWs nanorods has great influence on its optoelectronic properties, which would lead to different photodetecting performance. The spectral photoresponse of detectors with different diameters under the bias of 0.5 V at the room temperature is tested and the result is shown in Fig. 5*c*. It is obviously that four different fabricated InGaN/GaN QWs nanorods arrays detectors have different responsivity spectra and the responsivity decreased with the diameter of nanorods. In addition, the highest responsivity was obtained by 330 nm InGaN/GaN nanorods array. The 330 nm InGaN/GaN nanorods array detector had much better responsivity in the UV wavelength range of 350–370 nm, indicating good UV light detection sensitivity.

3.4. UV light detecting performance of InGaN/GaN nanorods array photodetector: As shown in Figs. 6*a* and *b*, the *I*–*V* curves of the InGaN/GaN nanorods array photodetector under dark and 365 nm UV light environment are measured. The four kinds of photodetectors are subjected to the applied bias of −5 to 5 V at room temperature while the resultant rectification properties of the typical p–n junction diodes are compared. The measured *I*–*V* characteristics at room temperature show a sharp reduction in a dark environment with the decrease of nanorods diameter in both the forward bias (0–5 V) and the reverse bias (−5 to 0 V). Under the 365 nm UV light illumination, the current of photodetectors almost has a similar amplitude in various InGaN/GaN nanorods array with different diameters. The decreased *I*–*V* characteristics are also observed in reverse bias (−5 to 0 V) as testing in a dark environment. The responsivity and detectivity of devices have been obtained and shown in Figs. 6*c* and *d*. The higher detecting performance with the smaller nanorods diameter is consistent with Figs. 6*a* and *b* at the 365 nm illumination, which indicates the excellent performance of 330 nm InGaN/GaN nanorods array. The time dependent photocurrent of the photodetector measured by periodically switching UV light is shown in Fig. 6*e*. There are approximately eight times the same current fluctuations and this indicates that the signal is repeatable. The response time curves are measured over one cycle of the UV light variation in order to investigate the response and recovery speed, and the results are given in Fig. 6*f*. It can be seen that the photocurrent can be rapidly and consistently switched between 'Off' and 'On' states at 0.5 V bias. The response time τ_r is defined as the rising time from 0 to 90% of maximum photocurrent that <0.2 s (beyond the resolution of the instrument), and the decay time τ_d, which defined as falling time from 100 to 10% of maximum photocurrent that measured as 0.4 s. It indicated that the response/

doi: 10.1049/mnl.2018.5160

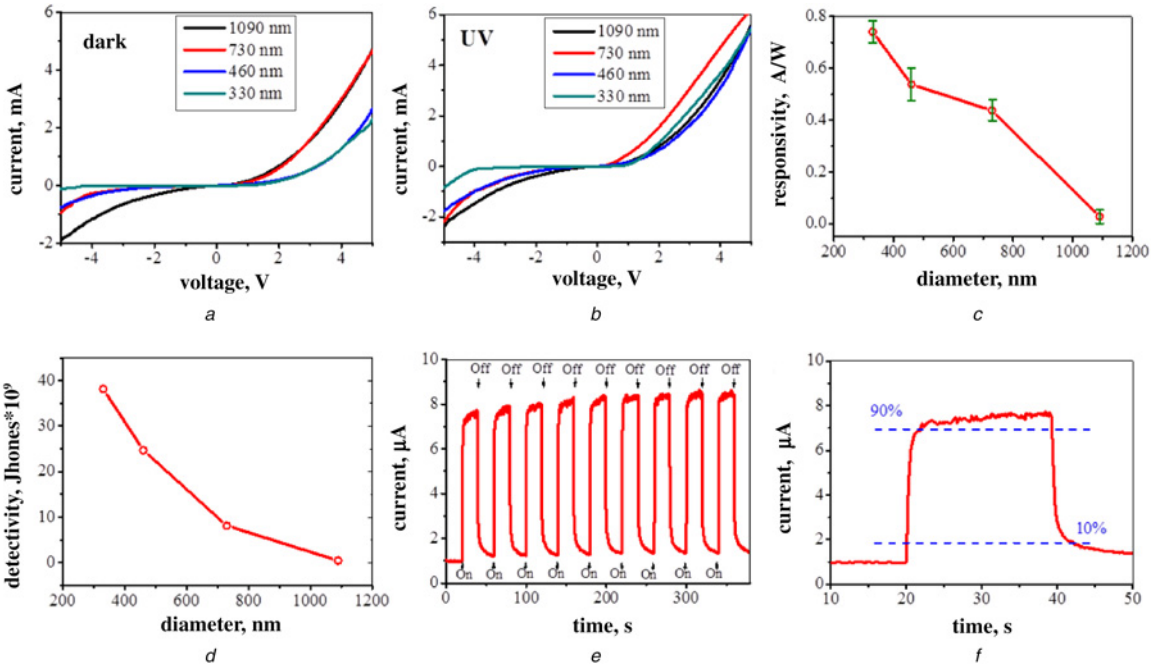

Fig. 6 *Current–voltage (I–V) characteristic of InGaN/GaN nanorods array photodetector of different diameters under*
a Dark condition
b 365 nm UV-light illumination
c, d Responsivity and detectivity as a function of incident power density, respectively
e, f Reproducible and one cycle on/off switching of the InGaN/GaN nanorods array photodetector at 0.5 V bias voltage by manually turning on and off the 365 nm UV-light illumination

Table 1 Comparison of the key parameters for different types of UV photodetectors

Materials	Wavelength, nm	Responsivity, A W^{-1}	Response/recovery time, s	Ref
core/shell InGaN/GaN QWs nanowire array	370	0.096	0.1	[20]
n-Ga:ZnO/p-GaN nanowire array	365	0.230	NA	[21]
GaN nanowire array	356	0.470	0.0025/0.022	[22]
single InGaN/GaN nanowire	370	0.160	0.46/10.8	[23]
ZnO nanowire array	370	0.180	0.67/1.02	[24]
TiO_2 nanowire array	350	0.27	1.23/0.6	[25]
GaN/ZnO nanorods	362	0.1389	1/1	[26]
InGaN/GaN QWs nanorods array	365	0.740	0.2/0.4	this work

recovery speed of the photocurrent is fast enough for the application. It was worth noting that the detector fabricated in this work exhibited better detecting performance compared to references, such as single InGaN/GaN QWs nanowire, ZnO nanowire array, TiO_2 nanowire array, GaN nanowire array, GaN/ZnO nanorods and core/shell InGaN/GaN QWs nanowire array [20–26]. As shown in Table 1, the responsivity of the InGaN/GaN nanorods array photodetector was found higher than in [20–26]. In addition, the InGaN/GaN nanorods array photodetector could detect UV light with faster response/recover time than ZnO nanowire array, TiO_2 nanowire array and single InGaN/GaN QWs nanowire [23–26]. Nonetheless, the response speed of the device is needed to further improve in the next in order to achieve an instantaneous response. In brief, the detector exhibited good response and fast response to UV light, which indicated that the InGaN/GaN nanorods array photodetector was a promising photo-detecting material.

3.5. UV light detecting mechanism of the InGaN/GaN nanorods array photodetector: As shown in Fig. 7, there is an MQW structure in InGaN/GaN nanorod, which generates an internal field. Therefore, there are excess carriers in the nanorod at room

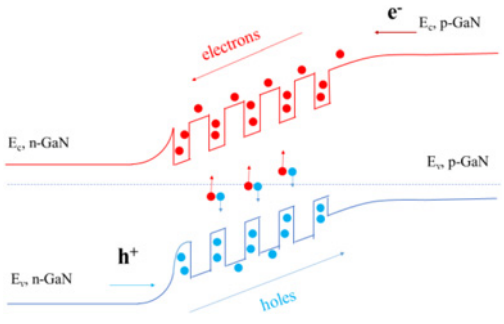

Fig. 7 *Schematic illustration of the energy band diagram of InGaN/GaN nanorods arrays*

temperature due to the internal field without light illumination. In dark conditions, these interfaces of MQWs become the energy barrier, which will impede the transportation of carrier. As the electrons transport across these barriers via tunnelling and thermionic emission, the emission current is extremely sensitive to barrier height modulation. The dark current of the

photodetector is inevitably high, which will limit the dynamic response range and detectability of the photodetector. There are two methods for improving the detectability of the photodetector, which increase the photocurrent or decrease the dark current. Usually, the excess photo generated holes are produced under UV illumination, resulting in a decrease in the barrier height and increase the photocurrent. However, as shown in Fig. 6*a*, the regulation of InGaN/GaN nanorod diameter can efficiently decrease the dark current. The diameter dependence of dark current is attributed to the increasing of resistance and the improving the surface area. Therefore, nanorods array photodetectors can exhibit higher response due to the two reasons.

4. Conclusion: In conclusion, vertically aligned InGaN/GaN nanorods array is prepared via a novel two-step etch approach, and the size of nanorods can be easily regulated in the range of 330–1090 nm by varying the etching parameters. The morphology characterisation results show that the nanorods are of straight and smooth appearance and the length of nanorods are about 4 μm. UV detectors based on nanorods array with different diameters are fabricated, and these devices exhibited fast response/recovery speed and good response. The UV detecting performance is found to be better with decreasing diameters. The unique detecting properties are attributed to the suppression of dark currents and the enlargement of the surface area. The fabrication of large scale vertically aligned InGaN/GaN nanorods array with controlled diameters will furtherly facilitates the various applications of GaN-based devices.

5. Acknowledgments: The authors greatly thank the financial supports from the National Natural Science Foundation of China (grant nos. 51572173, 51602197, 51771121 and 51702212), Shanghai Municipal Science and Technology Commission (grant nos. 15520720300, 16060502300, and 16JC402200), Shanghai Eastern Scholar Program (grant no. QD2016014) and Shanghai Pujiang Talent Program (grant no. 16PJ1407700). They sincerely thank Prof. Guang Wu in the East China Normal University for the help on the photoelectric test.

6 References

[1] Hayashi T., Kawase Y., Nagata N., *ET AL.*: 'Demonstration of electron beam laser excitation in the UV range using a GaN/AlGaN multi-quantum well active layer', *Sci. Rep.*, 2017, **7**, pp. 2944–2948

[2] Im J.S., Kollmer H., Off J., *ET AL.*: 'Reduction of oscillator strength due to piezoelectric fields in GaN/$Al_xGa_{1-x}N$ quantum wells', *Phys. Rev. B*, 1998, **57**, p. 9435(R)

[3] Lohr M., Schregle R., Jetter M., *ET AL.*: 'Quantitative measurements of internal electric fields with differential phase contrast microscopy on InGaN/GaN quantum well structures', *J. Phys. Status Solidi B*, 2016, **253**, pp. 140–144

[4] Zheng W., Huang F., Zheng R., *ET AL.*: 'Low-dimensional structure vacuum-ultraviolet-sensitive ($\lambda < 200$ nm) photodetector with fast-response speed based on high-quality AlN micro/nanowire', *Adv. Mater.*, 2015, **27**, pp. 3921–3927

[5] Koester R., Hwang J.S., Salomon D., *ET AL.*: 'M-plane core–shell InGaN/GaN multiple-quantum-wells on GaN wires for electroluminescent devices', *Nano Lett.*, 2011, **11**, pp. 4839–4845

[6] Nie B., Hu J.G., Luo L.B., *ET AL.*: 'Monolayer graphene film on ZnO nanorod array for high-performance Schottky junction ultraviolet photodetectors', *Small*, 2013, **9**, (17), pp. 2872–2879

[7] Dang V.Q., Trung T.Q., Kim D.I., *ET AL.*: 'Ultrahigh responsivity in graphene-ZnO nanorod hybrid UV photodetector', *Small*, 2015, **11**, (25), pp. 3054–3065

[8] Luo L.B., Zeng L.H., Xie C., *ET AL.*: 'Light trapping and surface plasmon enhanced high-performance NIR photodetector', *Sci. Rep.*, 2014, **4**, (1), pp. 3914–3921

[9] Liu Q., Liu B., Yang W., *ET AL.*: 'Alignment control and atomically-scaled heteroepitaxial interface study of GaN nanowires', *Nanoscale*, 2017, **9**, pp. 5212–5221

[10] Guo X.B., Fang X., Fu J.X., *ET AL.*: 'Study of nano-micrometer hybrid patterned substrates and their applications in semiconductor heteroepitaxy', *Opt. Instrum.*, 2014, **36**, pp. 20–25

[11] Tuo W.G., Hong R.J., Zhang D.W., *ET AL.*: 'The microstrcuture and optical propertied of Al, Sn doped ZnO thin film', *Opt. Instrum.*, 2015, **37**, pp. 278–282

[12] Reddy N.P., Shagufta N., Sudha M., *ET AL.*: 'Enhanced luminescence from GaN nanopillar arrays fabricated using a top-down process', *Nanotechnology*, 2016, **27**, p. 065304

[13] Liu X., Gu L.L., Zhang Q.P., *ET AL.*: 'All-printable band-edge modulated ZnO nanowire photodetectors with ultra-high detectivity', *Nature Commun.*, 2014, **5**, pp. 4007–4015

[14] Shi Y.F., Li Z.H., Feng B.C., *ET AL.*: 'Enhanced solar-blind ultraviolet single-photon detection with a Geiger-mode silicon avalanche photodiode', *Chin. Opt. Lett.*, 2016, **14**, p. 030401

[15] Lee J.W., Donohue J.F., Mackenzie K.D., *ET AL.*: 'Mechanism of high density plasma processes for ion-driven etching of materials', *Solid-State Electron.*, 1999, **43**, pp. 1769–1775

[16] Wang G.T., Li Q.M., Wierer J.J., *ET AL.*: 'Top–down fabrication and characterization of axial and radial III-nitride nanowire LEDs', *J. Phys. Status Solidi A*, 2014, **211**, pp. 748–751

[17] Yu F., Yao S.B., Römer F., *ET AL.*: 'Gan nanowire arrays with non-polar sidewalls for vertically integrated field-effect transistors', *Nanotechnology*, 2017, **28**, pp. 095206–095214

[18] Wang Q., Ji Z.W., Zho Y.F., *ET AL.*: 'Diameter-dependent photoluminescence properties of strong phase-separated dual-wavelength InGaN/GaN nanopillar LEDs', *Appl. Surf. Sci.*, 2017, **410**, pp. 196–200

[19] Chen W.J., Lin J.L., Hu G.H., *ET AL.*: 'Gan nanowire fabricated by selective wet-etching of GaN microtruncated-pyramid', *J. Cryst. Growth*, 2015, **426**, pp. 168–172

[20] Zhang H., Dai X., Guan N., *ET AL.*: 'Flexible photodiodes based on nitride core/shell p-n junction nanowires', *ACS Appl. Mater. Interfaces*, 2016, **8**, (39), pp. 26198–26206

[21] Yang L., Zhou H., Xue M.N., *ET AL.*: 'A self-powered, visible-blind ultraviolet photodetector based on n-Ga:ZnO nanorods/p-GaN heterojunction', *Sens. Actuators A, Phys.*, 2017, **267**, pp. 76–81

[22] Bugallo A.L., Tchernycheva M., Jacopin G., *ET AL.*: 'Visible-blind photodetector based on p-i-n junction GaN nanowire ensembles', *Nanotechnology*, 2010, **21**, (31), p. 7315201

[23] Zhang H., Guan N., Piazza V., *ET AL.*: 'Comprehensive analyses of core-shell InGaN/GaN single nanowire photodiodes', *J. Phys. D, Appl. Phys.*, 2017, **50**, p. 484001

[24] Guo L., Zhang H., Zhao D.X., *ET AL.*: 'High responsivity ZnO nanowires based UV detector fabricated by the dielectrophoresis method', *Sens. Actuators B, Chem.*, 2012, **166–167**, pp. 12–16

[25] Lahiri R., Ghosh A., Choudhuri B., *ET AL.*: 'Investigation on improved performance of erbium doped TiO_2 nanowire based UV detector', *Mater. Res. Bull.*, 2018, **103**, pp. 259–267

[26] Zhang L.C., Zhao F.Z., Wang C.F., *ET AL.*: 'Optoelectronic characteristics of UV photodetector based on GaN/ZnO nanorods p-i-n heterostructures', *Electron. Mater. Lett.*, 2015, **11**, pp. 682–686

doi: 10.1049/mnl.2018.5160